1	Effect of stoichiometry on the evolution of thermally
2	annealed long-range ordering in Ni-Cr alloys
3	
4	Fei Teng <sup>a,b</sup> , David J. Sprouster <sup>c</sup> , George A. Young <sup>a,d</sup> , Jia-Hong Ke <sup>a</sup> and Julie D.
5	Tucker a, *
6	<sup>a</sup> Materials Science Program, Mechanical Industrial Manufacturing Engineering Department,
7	Oregon State University, Corvallis, OR, 97331, USA
8	<sup>b</sup> Idaho National Laboratory, Idaho Falls, ID 83415, USA
9	<sup>c</sup> Department of Materials Science and Chemical Engineering, Stony Brook University, Stony
10	Brook, NY, 11794, United States.
11	<sup>d</sup> Kairos Power, Alameda, CA 94501.
12	
13	
14	Abstract
17	
15	Ni-based alloys, such as alloys 690 and 625, are widely used in the nuclear industry as
16	structural components, because of their desirable mechanical properties and resistance to stress
17	corrosion cracking. However, in some high chromium alloys, a disorder-order phase
18	transformation near 33 at.% Cr, is known to decrease ductility and fracture toughness. In this
19	study, the ordering transformation is investigated in Ni-Cr binary model alloys to better
20	understand the effects of composition. Model alloys with different stoichiometries (Ni/Cr = 1.8,
21	2.0, 2.2, 2.4) were isothermally aged up to 10,000 h at three temperatures (373°C, 418°C, and
22	475°C) and characterized by transmission electron microscopy (TEM), microhardness, and
23	synchrotron-based X-ray diffraction (XRD). TEM results show the evolution of the Ni <sub>2</sub> Cr
24	(MoPt <sub>2</sub> -type) ordered precipitates between 3,000 h and 10,000 h with corresponding size of ~10
25	nm to 20 nm. Microhardness testing results show that off-stoichiometry (Ni/Cr $\neq$ 2.0) alloys

- exhibit a smaller change with ordering compared to the stoichiometric (Ni/Cr = 2.0) alloy at all
- 2 temperatures. XRD quantifies ordering induced lattice contraction in the matrix structure and the
- 3 size of the ordered precipitates. No BCC Cr was detected by XRD or TEM during
- 4 characterization in the range of 29.83 to 35.66 at.% Cr after 10,000 h of aging, confirming that
- 5 all of the hardening can be attributed to the development of Ni<sub>2</sub>Cr in alloys ranging from Ni/Cr
- 6 of 1.8 to Ni/Cr of 2.4.

- 8 Keywords: Ni-based alloys, Long-range ordering, Synchrotron XRD, Microhardness,
- 9 Stoichiometry, Ni<sub>2</sub>Cr.

## 1 Introduction

High chromium, nickel-based alloys are widely used in various industrial fields, including nuclear, aerospace and the oil & gas industry. For Ni-Cr-based systems, 6XX type alloys with ~15 – 30 wt.% Cr (e.g., Alloy 600, 625, 690 and their weld filler metals) have been widely used in key components of light water reactors, due to the outstanding mechanical and chemical properties [1]. The strength, ductility, fracture toughness, and corrosion resistance, make Ni-based alloys desirable candidate materials for nuclear power plant components, such as reactor pressure vessel heads, core structural internals and steam generator tubing. The equivalent age hardenable alloys with ~15 – 20 wt.% Cr (e.g. X-750, 718 and 725) are widely used in rotor blades and wheels of gas turbines system, due to the corrosion, oxidation resistance, and high strength under high temperature environment [2]. Hastelloy C22 with ~22 wt.% Cr and ~13 wt.% Mo has been widely used under extreme corrosive environment due to the excellent resistance to corrosion and stress corrosion [3]. Despite their widespread industrial use, Ni-Cr (and Ni-Cr-Mo)

1 alloys can degrade if the Ni<sub>2</sub>Cr, long-range ordered (LRO) phase forms. Previous studies reveal 2 that an ordering transformation in Ni-Cr binary system occurs in a relative low temperature 3 region (300-590°C) around the Ni<sub>2</sub>Cr stoichiometry [4-8]. The formation of the Ni<sub>2</sub>Cr ordered 4 phase was demonstrated to have detrimental impacts on mechanical properties and lifespan of 5 structural components [9]. Previous research reveals that ordering has significant effects on the 6 mechanical properties including increasing hardness in Hastelloy C-22HS by Ni<sub>2</sub>(Mo,Cr) 7 ordered phase formation [10, 11], reducing fracture toughness [12], changing the fracture mode 8 in Ni-Cr and Ni-Cr-X model alloys by Ni<sub>2</sub>Cr [13], inducing internal stress in Nimonic 80A by 9 the lattice contraction associated with long range order [14], and increasing the susceptibility to 10 hydrogen embrittlement in superalloy C-276 by Ni<sub>2</sub>(Mo, Cr) formation after long term ageing 11 [15]. General effects of the LRO transformation include a decrease in lattice parameter [8, 16, 12 17] and change in slip mode [8]. Due to the significant degeneration caused by LRO, studies on 13 the kinetics of the ordering transformation have also been performed [18, 19]. The commercial 14 and model alloys, which are shown in Table 1, are the Ni-based alloys that have been 15 investigated for ordering in previous studies. Several commercial alloys are possibly located in 16 the ordering phase transformation field of the Ni-Cr phase diagram (30-35 at.% Cr range) as 17 reported by Marucco et al. [7] and Xiong et al. [5]. Table 1 provides the composition of some 18 commercial alloys that may be at risk of ordering in service at low temperatures [20]. 19 20 21 22 23

Table 1. Chemical composition of Ni, Cr, Fe of some commercial alloys (at.%).

Alloy	Ni	Cr	Fe	Ni/Cr	LRO Observed?	Reference
690	> 60.0	31.7-34.8	7.7-11.0	1.65-1.90	Yes	[21]
625	> 60.0	26.2-29.0	< 6.0	2.23-2.57	Yes	[21]
625+	70-74.0	25.2-29.0	<11.0	2.37-2.94	Yes	[21]
C22	66.5	29.5	3.7	2.25	Yes	[21]
X-750	72.77	18.14	8.44	4.01	No	[21]
718	56.42	22.28	31.30	2.53	No	[21]
725	63.83	26.92	9.25	2.37	Yes	[21]
FM52	>58.56	30.34	7.08-12.01	1.89-2.18	No Result	[22]
WE152	>62.52	30.4	7.08-12.01	1.89-2.06	No Result	[22]
80A	74.9	21.9	3.07	3.42	Yes	[14]
Ni2-Cr	~66	~33	< 0.01	~2.0	Yes	[12, 23]
Ni3-Cr	~75	~25		~3.0	Yes $\frac{(Ni_2Cr + \alpha' Cr)}{(Ni_2Cr + \alpha' Cr)}$	[23]
Ni2-Cr-Fe	61.8-66.98	30.3-32.05	1-9	~2.0	Yes	[13]

2

3 The Ni<sub>2</sub>Cr ordered phase has been identified as MoPt<sub>2</sub>-type precipitates with Immm 4 symmetry [13, 20, 24-26]. Figure 1 shows the MoPt<sub>2</sub> ordering superlattice structure in the Ni-Cr 5 system. Under the reference lattice of face-centered cubic (FCC) structure, ordered Ni<sub>2</sub>Cr phase 6 is of body-centered orthorhombic (BCO) structure and fully coherent with FCC matrix. During 7 the ordering transformation of Ni-Cr system, atoms reorganize from random solid solution into 8 regular patterns [27]. The ordered phase will nucleate and grow when the composition falls 9 within the ordered phase region or in a two-phase region (e.g., BCC Cr + Ni<sub>2</sub>Cr) [6-8, 23, 28]. 10 The phase stability can be heavily dependent on stoichiometry and temperature, but the 11 same kinetics appear to govern both stoichiometric and off-stoichiometric alloys as long as LRO 12 forms. The ordered phase has a Ni/Cr ratio of 2, however, the width of the ordered domain is 13 poorly defined due to the challenge of collecting low temperature data. For Ni-Cr binary alloys, 14 Young et al. and Karmazin et al. reported the optimal rate of ordering occurs at ~475°C [20, 29].

- 1 Fe additions tend to lower the nose of the TTT curve, making it harder to accelerate testing in
- 2 Ni-Cr-Fe ternary system [20, 30, 31]. In the Ni-Cr-Mo ternary system, Mo additions raise the
- 3 ordering critical temperature [32] as reported by Arya et al. and stabilize the ordered phase at
- 4 higher temperatures according to Karmazin et al. [33]. Delabrouille et al. reported ordering in
- 5 Inconel 690 after a 70,000 h heat treatment at 420°C via the evolution of microhardness and
- 6 TEM characterization [4]. Irradiation was also found to enhance the ordering rate significantly
- 7 for both model alloys and commercial alloys. Frely et al. reported ordering kinetics in Ni-Cr-Fe
- 8 model alloys can be enhanced in orders of magnitude by 2.5 MeV electron irradiation [30, 31].
- 9 In the research of Song et al., six of the twelve commercial alloys (including C22, 690, 625,
- 10 625+, 725, etc.) were found to produce the Ni<sub>2</sub>Cr LRO via TEM dark field imaging when
- irradiated using 2 MeV proton at 360°C with 2.5 dpa damage level [21].
- Due to the lower critical temperatures in Fe containing commercial alloys [30], binary Ni-
- 13 Cr alloys have often been used to clarify the behavior and influence of ordering. In previous
- research on binary Ni-Cr alloys, the hardening effect can be observed by measuring
- microhardness. A linear relationship between Vickers microhardness and yield strength was
- reported by Young et al. in Ni-33 at.% Cr binary alloy, which was isothermally heat treated at
- 17 475°C for up to 10,000 h [13]. The effect of ordering transformation on crack growth of Ni<sub>2</sub>Cr
- binary alloy has been explored in previous research of Pao et al., which indicates that fatigue
- crack growth rate decrease and crack growth thresholds increase with the extent of ordering [34].
- 20 Ordered precipitates can be qualitatively characterized by both indirect methods, such as
- 21 microhardness [23, 35, 36], and direct methods, such as atom probe tomography (APT) [37, 38],
- 22 TEM [20, 39], and synchrotron X-ray diffraction (XRD) [35]. However, a systematic
- 23 quantitative study on the evolution of LRO has not been performed due to the difficulty on

1 quantifying the ordered phase fraction and the relationship with mechanical properties even with

2 advanced characterization techniques such as TEM and APT. There is little experimental data in

this region (29-36 at.% Cr, T = 373°C-475°C) to confirm the extent of the ordered phase at

different temperatures and different stoichiometry from previous research. The role of

stoichiometry in Ni<sub>2</sub>Cr binary alloys and Ni-Cr-Fe ternary alloys (30-67 at.% Ni, 17-32 at.% Cr,

and 1-51 at%. Fe) has been studied by Marucco between 450 and 600°C [7, 28]. However, both

studies did not cover the most common service temperature in the piping system of light water

reactors (300 to 400°C).

In this study, four compositions of Ni-Cr alloys (30-36 at.% Cr) were aged at three temperatures (373°C, 418°C, 475°C) for up to 10,000 h. TEM characterization was performed to reveal the evolution of Ni<sub>2</sub>Cr ordered precipitation in the microstructure. Then, Berkovich microhardness was used to measure the ordered phase induced increasing on microhardness as function of temperature and stoichiometry. Finally, XRD was used to characterize the evolution of ordered precipitates and matrix including phase fraction, lattice parameter, size of ordered phase, and internal strain. The purpose of this work is to explore the relationship between extent of ordering, ageing temperature, and stoichiometry in Ni-Cr binary system at low temperature range to contribute the lifetime prediction modeling in Ni-based commercial alloys.

## Experimental Methods

# 20 2.1 Fabrication of model alloys

21 The Ni-Cr binary model alloys were fabricated by small batch (~300g) arc-melting, then

all samples are water-quenched to room temperature. Samples were made in stoichiometry ratios

hot-rolled into plates, and homogenized in a furnace for 24 h at 1093°C. After homogenization,

1 of Ni/Cr (at.%) of 1.8, 2.0, 2.2, and 2.4, which follows the unknown region of the Ni-Cr phase 2 diagram under 500°C from previous research [5]. Compositional analysis was performed by a 3 third-party test laboratory. The analytical method is based on CAP-017N inductively coupled 4 plasma multi-element inorganic analysis (ICP-AES) and ASTM 1019-11 (Comb./IGF): standard 5 test methods for determination of C, S, N, and O in steel, Fe, Ni, and Co alloys by various 6 combustion and fusion techniques. The actual composition results are shown in Table 2. The 7 rolled plates were cut into 10×10×5 mm<sup>3</sup> specimens by electrical discharge machining, which 8 minimizes heat generation and the corresponding interpretation on microstructure during cutting. 9 Next, specimens were isothermal heat-treated at three temperatures (373, 418 and 475°C) for up 10 to 10,000 h. Each furnace has three thermocouples that measure the temperature around samples 11 and the whole ageing system is monitored by a LabView program combined with National 12 Instrument cDAQ-9171 chassis and NI-9214 temperature input module. All thermal couples are 13 calibrated by Fluke 9142 Field Metrology Wells. The reference temperature is measured from 14 5610 Fluke Temperature Probes. All samples are cooled by water quenching to room 15 temperature after aging. The heat treatment matrix is shown in Table 3.

Table 2. Composition of binary model Ni-Cr Alloys (at.%). Values of Ni/Cr are used in following to clarify stoichiometry.

Element	Ratio 1.8	Ratio 2.0	Ratio 2.2	Ratio 2.4
C	0.05	0.05	0.05	0.05
Cr	35.66	33.24	31.10	29.83
Fe	0.010	0.010	0.010	0.010
P	0.013	0.011	0.011	0.011
S	0.004	0.004	0.004	0.002
Ni	64.27	66.69	68.83	70.10
Ni/Cr	1.80	2.01	2.21	2.35

16

Table 3. Heat treatment matrix of model Ni-Cr alloys. One sample from each stoichiometry is included in each time/temperature group.

Time (h)	500	1,000	3,000	5,000	10,000	
Temperature (°C)						
373	4	4	4	4	4	
418	4	4	4	4	4	
475	4	4	4	4	4	

#### 2.2 TEM

After aging, specimens to be characterized by TEM were first sectioned by low speed diamond saw into  $\sim$ 1 mm thick slices. The slices were then ground to thin foil with the thickness less than 120  $\mu$ m with 1200 grit SiC sandpaper finished surface on both sides. The foils were punched into 3 mm diameter disks and jet electro-polished in 20% HClO<sub>4</sub> – 80% CH<sub>3</sub>OH at - 40°C and 15V using a Struers Tenupol 5 with a Julabo FP50 closed-cycle refrigeration system. TEM characterization was performed by using the FEI Tecnai TF30-FEG transmission electron microscope located in Center for Advanced Energy Studies (CAES) at 300 kV voltage. To best reveal the size of precipitates, the [112] zone axis was selected for dark field imaging.

## 2.3 Microhardness

For microhardness tests, the bulk specimens (in dimension of  $10\times10\times5$  mm³) were polished using SiC papers from 240 to 800 grit followed by 0.05 µm alumina polishing. Microhardness measurements were performed by using MicroMaterials NanoTest Vantage nanoindenter with a Berkovich diamond tip and a load of 500 mN. The load was chosen to balance degradation of indenter tip, sensitivity for vibration from environment during testing, resistance on effect of grain orientation, effect of grain boundary on indentation, and the accuracy level of the result. A larger load causes faster tip damage, which changes the dynamic

1 area function that is used to calculate microhardness. A smaller load requires lower

2 environmental vibration. Considering these effects on standard deviation of measurement,

3 microhardness measurements using a grid of (4×5) were performed twice (total 40 indents) on

the sample surface with 600 µm between indentations in each direction. Considering the effect of

grain orientation and grain boundary on data variance, all 40 data points are ranked from low to

high and the lowest 10 and highest 10 points were removed from the data set. Only the remained

middle 20 data points were analyzed for hardness.

## 2.4 Synchrotron X-ray diffraction (XRD)

XRD measurements were performed using the high-energy X-rays available the X-ray Powder Diffraction beamline of the National Synchrotron Light Source-II (NSLS-II) [40, 41]. All measurements were performed in transmission mode with an amorphous silicon-based flat panel detector (Perkin-Elmer) mounted orthogonal to and centered on the beam path. The sample-to-detector distances and tilts of the detector relative to the beam were refined using a LaB6 powder standard (NIST standard reference material 660c). The wavelength of the incident X-rays was 0.2370 Å (52.3149 keV). The sample-to-detector distance was calculated to be 1351.94 mm. Samples were continuously rotated during acquisition to improve the powder averaging. Multiple patterns were collected to avoid saturation of the detector. Typical count times were 0.5-1 sec (depending on the sample). All raw two-dimensional patterns were background corrected by subtracting the dark current image and any air scattering. Noticeable artefact regions of the detector (like the beam stop, dead pixels) were masked. The corrected and masked two-dimensional detector images were then radially integrated to obtain the one-

dimensional powder diffraction patterns. The background subtracted XRD patterns were

2 Rietveld refined with the TOPAS software package (BRUKER). The peak profiles were modeled

3 by a modified pseudo-Voigt function. The instrument contribution to the broadening of the

measured profiles was quantified by fitting a LaB<sub>6</sub> NIST powder standard, with known

crystallite-domain size and negligible strain contribution. The Gaussian and Lorentzian-based

instrument broadening parameters were subsequently fixed during the analysis of the alloys

under investigation.

Table 4 shows the test matrix for XRD characterization. To best reveal the evolution of ordered phase, Ni/Cr = 2.0 samples aged at 475°C were chosen to perform the test. Ni/Cr = 2.0 samples aged at 373°C and 418°C for 10,000 h were also tested for exploring the role of temperature in ordering transition. Moreover, Ni/Cr = 1.8, 2.2, and 2.4 samples were chosen to reveal the evolution of ordering as a function of stoichiometry.

Table 4. Test matrix for XRD. Tested stoichiometry is shown in each table cell.

Time (h) Temperature (°C)	500	1,000	3,000	5,000	10,000		
373					2.0		
418					2.0		
475	2.0	2.0	2.0	2.0	1.8, 2.0.		
4/5	2.0	2.0	2.0	2.0	2.2, 2.4		

#### 3 Results

1

2 3.1 Transmission electron microscopy

3 Figure 2 shows the evolution of MoPt<sub>2</sub>-type ordered precipitates with time snapshots of 4 3,000 h, 5,000 h, and 10,000 h ageing at 475°C in [112] zone axis. In dark field mode, both  $\frac{1}{3}$  [220] and  $\frac{1}{3}$  [13 $\overline{1}$ ] spots were captured for Figure 2(a). The  $\frac{2}{3}$  [311] and  $\frac{2}{3}$  [220] spots were 5 selected for Figure 2(b) and 2(c). 6 7 The selected-area electron diffraction patterns indicate the existence of the ordered phase 8 after isothermal ageing and the corresponding dark field images reveal the distribution of Ni<sub>2</sub>Cr-9 ordered precipitates in samples. TEM dark field images generally reveal the evolution of 10 ordering transition in quality as ageing going. After 3,000 h ageing (Figure 2(a)), small ordered 11 precipitates can be observed, and some precipitates start growing into an early stage superlattice 12 structure with a size ~10 nm. As ageing continues, ordered precipitates with larger coherent particle size (p-size) of ~13 nm can be observed after 5,000 h isothermal heat treatment and the 13 14 superlattice structure is more obvious (Figure 2(b)). P-size keeps growing to ~20 nm as ageing 15 time reaches 10,000 h (Figure 2(c)). The superlattice structure of thermal induced Ni<sub>2</sub>Cr ordered 16 structure can be observed in some area clearly. Figure 2 shows that the boundary between 17 precipitates appears clearer with increasing aging time. No clear precipitates can be observed in 18 Figure 2(a) (3,000 h). Dark area between precipitates start showing in Figure 2(b) (5,000 h) and 19 precipitates can be imaged clearly in Figure 2(c) (10,000h). However, it is difficult to calculate 20 ordered phase fraction from TEM darkfield images because of the low contrast between matrix 21 and ordered precipitates. More precise, robust, and larger volume characterization method, such

as synchrotron XRD, is needed to determine the ordered phase fraction.

## 3.2 Microhardness

1

2

3

4

5

6

7

8

9

10

11

12

13

14

15

16

17

18

19

20

21

22

23

We define embrittlement here as the difference of Berkovich microhardness at current ageing time (GPa) and the microhardness of same sample at as-received condition (GPa). The average change in Berkovich microhardness, which is the difference of microhardness before and after isothermal ageing, from 500 to 10,000 h isothermal heat treatment as function of stoichiometry at three temperatures are shown in Figure 3. The result shows that the relationship of embrittlement at three temperatures is generally 475°C > 418°C > 373°C during the whole ageing time. In the first 500 and 1,000 h ageing, the change in microhardness as a function of temperature is  $475^{\circ}\text{C} > 418^{\circ}\text{C} > 373^{\circ}\text{C}$ . The change on microhardness as a function of stoichiometry at 475°C is  $2.0 \approx 2.2 > 1.8 \approx 2.4$ . The role of stoichiometry at 418°C and 373°C on the change of hardness is not obvious; the four stoichiometries reveal similar microhardness changes at both temperatures. When the ageing time extends after 3000 h, role of stoichiometry starts to become more obvious at 475°C. The relationship of embrittlement as a function of stoichiometry is  $2.0 > 2.2 \approx 1.8 > 2.4$  at 475°C. This relationship keeps stable at 418°C compared to the relationship before 1000 h. For the change of microhardness at 373°C, the 2.2 sample is of slightly higher hardness than other compositions. Compared to the embrittlement before 1,000 h, no obvious change in the relationship of embrittlement can be observed at 373°C. However, the degree of embrittlement, which is between 0.3 and 0.75 GPa, is much larger than that of 500 h and 1,000 h, which is between 0 and 0.25 GPa. When the ageing time equals to 10,000 h, the relationship of microhardness at all temperatures is close to  $2.0 > 2.2 \approx 1.8 > 2.4$ . The change of microhardness at 475°C of the samples aged for 10,000 h is similar to that of 3,000 h and 5,000 h. For 418°C, the embrittlement increases to 1 GPa at all stoichiometry, which is larger than

5,000 h. For 373°C, the change of microhardness is of obvious increasing compared to that of
 5,000 h.

The size of nanoindentation is ~20  $\mu$ m, which is smaller than the grain size (~150  $\mu$ m). The size difference may cause the measurement of microhardness is heavily dependent on grain properties, such as grain orientation. Previous research [42] shows that the yield strength varies in different grain orientation measured by micro pillar compression in Ni<sub>2</sub>Cr model alloys. To minimize the interruption, ranking-and-choosing method in data analysis that mentioned in previous section of this paper was used. The uncertainty revealed in the hardness measurement indicates that microhardness needs to be combined with another more reliable technique to clarify the evolution of ordering as a function of temperature and stoichiometry.

## 3.3 Synchrotron X-ray Diffraction

Considering the challenge of measuring ordered phase fraction by TEM and grain properties influenced microhardness, XRD is the ideal technique to precisely quantify the evolution of ordered precipitation. Also, previous research from Gwalani et al. [35] shows the efficiency of XRD on identifying ordered precipitates.

The XRD patterns shown in Figure 4 (phases are included for references) confirm the formation of the Ni<sub>2</sub>Cr ordered phase. All samples show the cubic FCC Ni-Cr matrix (higher peaks indicated by the blue tick marks). All samples, with the exception of the "as-received" sample, show peaks from the orthorhombic phase Ni<sub>2</sub>Cr (red tick marks). The peaks from the Ni<sub>2</sub>Cr phase vary in height and width between samples due to varying concentration and coherent particle size (p-size). There does not appear to be any diffraction peaks for BCC Cr in the current samples. In Figure 4(a), compared to as-received 2.0 sample, both 2.0-475-5000 and

1 2.0-475-10,000 samples show Ni<sub>2</sub>Cr diffraction and the corresponding intensity increases with 2 ageing time, as confirmed by quantitative analysis (Table 5). Figure 4(b) reveals diffraction 3 patterns that confirm the formation of the Ni<sub>2</sub>Cr ordered phase in all four stoichiometries. Figure 4 4(c) shows the diffraction pattern from samples with different ageing temperatures (373°C, 5 418°C, and 475°C). Significant peak broadening can be observed in the Ni<sub>2</sub>Cr precipitates at 6 lower temperatures, indicative of small precipitate sizes. The lattice parameters (and volume of 7 unit cell) also appear to be temperature dependent and increase with increasing temperature. 8 The structural results from the Rietveld fitting are shown in Table 5 and Figure 5 for the 9 phase fraction, lattice parameter (for both matrix and precipitates), size of ordered precipitation 10 (p-size) and strain (numbers in parentheses () are errors from the refinements). The blue (dash 11 line) plot of Figure 5 shows the evolution of p-size as a function of ageing time for Ni/Cr = 2.0 12 samples aged at 475°C. The p-size increases rapidly in the beginning period of heat treatment 13 then starts slowing down after 1,000 h. A similar but reversed trend can be observed on the change of lattice parameters in same sample as shown in the green (dots line) plot in Figure 5. 14 15 The matrix lattice parameter contracts rapidly in the beginning 1,000 h from 3.567 Å, and then 16 plateaus around 3.558 Å. The pink (dash-dot line) plot in Figure 5 shows the evolution of 17 ordered phase fraction. Different from the tendency of other parameters, the ordered phase 18 fraction goes to  $\sim 6\%$  rapidly (at 500 h) and keeps going down till 5,000 h. The ordered phase 19 fraction keeps stable at ~5% after 5,000 h. The black (solid line) in Figure 5 shows the evolution 20 of microhardness on the same samples for comparison. Figure 6 shows change of the strain on 21 Ni/Cr = 2.0 jet-polished samples from 3,000 h to 10,000 h. A significant jump on strain can be 22 observed between 5,000 h and 10,000 h. Figure 7 shows the evolution of strain, p-size, and

change in microhardness as a function of stoichiometry. The Ni/Cr = 2.0 and 2.4 samples have

- 1 the largest and smallest values on all parameters correspondingly, which means the farther
- 2 distance from 2.0, the smaller p-size/strain/change in microhardness can be observed in the
- 3 sample. Ni/Cr = 1.8 sample is of slightly larger size on precipitates than Ni/Cr = 2.2.

5 Table 5. Summary and comparison of Rietveld refinements.

	Table J.	Summal,	y and com	12011	or Kictve	a remit	mento.	Phase					
sample	phase	a (Å)	(±)	b (Å)	(±)	c (Å)	(±)	Fraction (%)	(±)	p-size (nm)	(±)	strain	(±)
2.0 As- received	Fm-3m	3.56720	(0.00005)									0.28	(0.01)
2.0-500hr-	Fm-3m	3.56031	(0.00013)									0.23	(0.02)
475°C	Immm	2.50639	(0.00696)	7.52024	(0.02264)	3.59554	(0.00638)	6.0	(0.2)	9	(0.5)		
2.0-1000hr-	Fm-3m	3.55875	(0.00010)									0.39	(0.01)
475°C	Immm	2.50923	(0.00253)	7.50987	(0.00845)	3.59472	(0.00258)	5.8	(0.2)	12.9	(1.0)		
2.0-3000hr-	Fm-3m	3.55860	(0.00016)									0.24	(0.02)
475°C	Immm	2.50747	(0.01200)	7.53310	(0.03940)	3.56688	(0.01598)	5.6	(0.69)	12.4	(2.0)		
2.0-5000hr-	Fm-3m	3.55853	(0.00009)									0.23	(0.01)
475°C	Immm	2.50323	(0.00834)	7.50819	(0.02548)	3.60427	(0.00721)	4.7	(0.2)	15.0	(2.0)		
2.0-10,000hr-	Fm-3m	3.55790	(0.00010)									0.54	(0.01)
475°C	Immm	2.50816	(0.00311)	7.50204	(0.00940)	3.59506	(0.00239)	4.9	(0.2)	19.0	(1.1)		
1.8-10,000hr-	Fm-3m	3.56387	(0.0001)									0.50	(0.011)
475°C	Immm	2.51294	(0.00213)	7.5324	(0.00659)	3.5855	(0.0023874)	6.0	(0.3)	15	(2)		
2.2-10,000hr-	Fm-3m	3.55598	(0.00013)									0.47	(0.01)
475°C	Immm	2.50852	(0.00240)	7.51625	(0.00910)	3.58372	(0.00250)	12.1	(0.5)	12.7	(1.0)		
2.4-10,000hr-	Fm-3m	3.55570	(0.00012)									0.39	(0.01)
475°C	Immm	2.51187	(0.00480)	7.57838	(0.01850)	3.57230	(0.00540)	6.8	(0.5)	8.0			
2.0-10,000hr-	Fm-3m	3.56158	(0.00010)									0.24	(0.01)
373°C	Immm	2.48545	(0.01000)	7.52002	(0.03100)	3.63926	(0.00800)	6.6	(0.2)	4.0			
2.0-10,000hr-	Fm-3m	3.55954	(0.00009)									0.29	(0.01)
418°C	Immm	2.50636	(0.00637)	7.52694	(0.02159)	3.59439	(0.00592)	9.5	(0.3)	6.7	(1.0)		

## 4 Discussion

1

2

4.1 Evolution of ordered precipitation in isothermal aged Ni-Cr binary system

3 The XRD and TEM results reveal the evolution of ordered precipitation among Ni/Cr = 2.04 samples. Ni/Cr = 2.0 samples are used here to qualify and quantify the evolution of thermal 5 ageing induced ordering and to confirm the reliability of microhardness result in all samples as 6 the microhardness starts showing saturation behavior. Figure 5 shows the comparison between 7 the evolution of p-size, lattice parameter, ordered phase fraction, and microhardness as function 8 of time. For the 2.0 sample aged at 475°C, the XRD result shows that the evolution of the matrix 9 lattice parameter, size of ordered particle, and microhardness reach saturation after 1,000 h 10 ageing. This tendency agrees with each other between the parameters except ordered phase 11 fraction. The XRD measured p-size trend concurs with the results of TEM characterization 12 (Figure 2), which indicates a significant increase in precipitate size from 5,000 h to 10,000 h 13 (Figure 5). 14 Compared to the most recent TEM characterization from Song et al. [21] on irradiated 15 commercial alloys, the p-size of this study here are significantly smaller. The phase fraction and 16 p-size is also smaller compared to the samples with high Mo content in the research of Verma et 17 al. [36] due to the ordering rate enhancement of Mo in Ni-Cr system, which was calculated via 18 TEM darkfield imaging. Previous researchers have shown that the addition of Mo, Nb, and W is 19 able to stabilize ordered precipitates at higher temperatures [33, 43, 44]. In previous research on 20 Ni-Cr model alloys, only small precipitates are considered to be LRO precipitate in dark field 21 mode. By condensing the electron beam in dark field mode, the dark field image with uneven 22 intensity reveals both small precipitates and surrounding grey region (Figure 2(a)). The grey 23 area, which contains both small precipitates with weak intensity and some matrix material, can

- be removed by adjusting image contrast and brightness. The superlattice structure from LRO
- 2 Ni<sub>2</sub>Cr precipitates is visible after 3,000 h of ageing in Figure 2(a). As ageing continues, the
- 3 ordered precipitates start unifying into superlattice structures (Figure 2(b)). In Figure 2(b) and
- 4 2(c), the p-sizes are  $\sim 10$  nm and  $\sim 10-20$  nm, which is in rough agreement with the measurement
- of p-size by XRD (15  $\pm$  2 nm and 19  $\pm$  1.1 nm correspondingly). Therefore, the evolution of
- 6 LRO precipitation can be observed as a growth process based on the result of TEM
- 7 characterization in Figure 2.
- 8 In previous work by Marucco et al. [8], the change of lattice parameter is considered a
- 9 direct effect of LRO. Combined with the lattice contraction measured by XRD (Figure 4(a)), all
- 10 samples characterized by TEM, which are 2.0-475°C-3,000 h, 2.0-475°C-5,000 h, and 2.0-
- 11 475°C-10,000 h, are in the ordering saturation region. Lattice parameter of matrix stabilizes at
- 12 3.558 Å from the original values of 3.567 Å (Figure 4(c)), which is 0.25% lattice contraction
- measured by lab XRD and reported to be the lattice constant value of saturation of ordering in
- Ni-Cr binary system by Marucco et al. [8, 23]. The lab XRD lattice parameter results are also in
- 15 good agreement with the results from Gwalani et al. [35], which was measured by synchrotron
- 16 XRD on Ni-33 at.%Cr model alloy.
- 17 P-size increases with ageing time and no saturation can be observed during the times and
- temperatures investigated in this study, but only a slower rate of increase can be observed from
- the XRD data (Figure 5). The tendency indicates p-size is of a significant growth between 5,000
- 20 h and 10,000 h while the ordering induced lattice contraction effect, ordered phase fraction and
- 21 microhardness is stabilizing after 5,000 hours as shown in Figure 5. To reveal the other effect of
- p-size, strain was calculated from XRD in 3,000 h, 5,000 h, and 10,000 h jet polished TEM disks
- 23 to minimize the effect of external induced strain in the result of calculation (Figure 6). Result

- shows the significant increase in strain from 5,000 h to 10,000 h (from 0.23 to 0.54), which
- 2 indicates that the internal strain may be induced by increasing p-size instead of an increase in the
- 3 ordered phase fraction or the net lattice contraction.

## 4.2 Effect of phase fraction and p-size on hardening

For Ni/Cr = 2.0 samples at 475°C, the similarity between p-size, lattice parameter, and microhardness (Figure 5) indicate the strong relationship between the size of ordered particle, ordering induced lattice contraction and the corresponding hardening effect. The evolution of ordered phase fraction in Figure 5, however, shows a different behavior from other ordering induced parameters. Ordered phase fraction reaches ~6% by 500 h of ageing, slowly decreases to ~5% from 500 h to 5,000 h. Then the ordered phase fraction steadily remains at ~5% from 5,000 h to 10,000 h. The decreasing behavior may cause by the changing of precipitates from short range ordering (SRO) to long range ordering (LRO). The coexisting of SRO and LRO may confound the quantification of XRD on phase fraction. The saturation of ordered phase fraction (at ~500 h) happened earlier than other parameters (at ~1,000 h). By combining the result of p-size and ordered phase fraction, we can have a rough idea about the morphology change during the evolution from SRO to LRO: small ordered precipitates are distributed high density at the early stages of aging, then grow into larger, lower-density oblate spheroidal precipitates at the later stage of ageing.

For Ni/Cr = 2.0 samples at 373°C and 418°C, considering the relationship between ordering and the corresponding embrittlement effect in Ni-Cr system, the increase in microhardness can be trusted to indicate degree of ordering indirectly [8, 26, 35, 36, 45].

However, the degree of long range ordering not the combination of SRO and LRO that correlates

1 microhardness based on the XRD result in this study and more detail will be given later. During 2 the analysis of phase fraction data on 1.8-10,000-475, 2.0-10,000-475, 2.2-10,000-475, and 2.4-3 10,000-475, it should be noticed that 2.2-10,000-475 is of the highest phase fraction value, which 4 does not fit the relationship of microhardness. The trend of hardening (Figure 3) indicates that 5 microhardness will reach nearly saturation after 1,000 h isothermal ageing at 475°C, whereas the 6 time to reach saturation for 418 and 373°C will be longer than 10,000 h. Considering the 7 embrittlement behavior of 418°C and 373°C have not reached equilibrium, the saturation 8 microhardness cannot be determined these temperatures. The effect of stoichiometry on ordering 9 is characterized by microhardness at all three temperatures (373°C, 418°C, and 475°C), and by 10 synchrotron XRD for all stoichiometry aged for 10,000 h at 475°C. As shown in Figure 7, the 11 effects of stoichiometry on ordering transformation in aspects of internal strain, precipitation 12 size, and microhardness are identical  $(2.0 > 2.2 \approx 1.8 > 2.4)$ , which is different from that of phase 13 fraction (2.2 > 2.4  $\approx$  1.8 > 2.0) from Table 5. The result indicates that the effect of phase fraction 14 should be considered differently from internal strain and precipitation size. 15 Both size of precipitates and volume phase fraction is another critical parameter of precipitation strengthening mechanism. The role of precipitation's volume fraction varies in 16 17 different hardening mechanisms as each mechanism is calculated under specific condition [46]. 18 Orientation and strain rate dependence is another complication for the application of mechanisms 19 on the Ni-based alloys containing high precipitation volume fraction. With the influence of 20 particle size, the overall hardening effect can be very complex. It is difficult to clarify hardening 21 based on precipitation size or volume fraction alone, which explains the different behavior 22 between ordered phase fraction and microhardness of Ni-Cr model alloys in this research.

23

## 4.3 KJMA Analyses on microhardness as a function of stoichiometry

For analyzing the isothermal hardening kinetics, the Kolomogorov-Johnson-Mehl-Avrami (KJMA) equation was used to describe the data [47]. The fitting on microhardness data has been widely used in previous studies to describe hardening as a function of time and temperature [48-52]. Stoichiometry and temperature are two key parameters of interest for the Ni<sub>2</sub>Cr ordering transformation, indicated by the data presented in Figure 7 and Figure 8, respectively. To characterize the role of stoichiometry and temperature on microhardness as a function of time, equation fitting was performed, and the fitted parameters are compared with that of previous studies.

In the KJMA equation (6), f is the fraction of transformed structure among matrix, which is assumed to be directly proportional to the change in hardness, t is the ageing time (h), and n is the Avrami exponent. The Arrhenius form of k shown in equation (7), where  $k_0$  is a constant, Q is the apparent activation energy, R is the gas constant (8.314 J/mol.K), and R is the ageing temperature in Kelvin. Based on the previous fitting work on microhardness and lattice parameter from Young et al. [13, 20], equation (6a) approximates the phase fraction in terms of changes in microhardness. Where R0 is the initial microhardness, R1 is the microhardness at saturation and R2 is the microhardness at a particular combination of ageing time and temperature. Off-stoichiometry samples (R3 is a particular combination of ageing time and temperature to the stoichiometric sample (R3 is the transformation saturates.

$$f = 1 - e^{kt^n} \tag{6}$$

$$f = \frac{H - H_0}{H_{Max} - H_0} \tag{6a}$$

$$k = k_0 e^{-Q/RT} \tag{7}$$

1 The result of KJMA fitting on microhardness is shown in Figure 9. The fitting parameters used here are:  $k_0 = 3.00E + 05 \text{ h}^{-1}$ , Q = 120 kJ/mol, n = 0.75. The  $H_{\text{Max}}$  values for 1.8, 2.0, 2.2, and 2 3 2.4 stoichiometry are 1.75, 2.5, 2, and 1.7 correspondingly. The parameters agree with previous 4 fitting result ( $k_0 = 3.50E + 07 \text{ h}^{-1}$ , Q = 147 kJ/mol, n = 0.65) on the similar samples and ageing 5 conditions from Young et. al [20]. Here, the apparent Q and Avrami exponent, n, are consistent 6 with previous studies Q ~ 120 kJ/mol indicative that classical bulk diffusion does not control 7 hardening rate but some alternate process such as vacancy hopping likely does. 8 As shown in Figure 9, the Cr-rich (Ni/Cr = 1.8) and stoichiometric (Ni/Cr = 2.0) alloys are 9 reasonable well fit by the KJMA equation with the apparent activation energy (Q~120 kJ/mol) 10 capturing the increased time needed to produce hardening at decreased temperature. As 11 previously discussed, the plateau in hardness is an estimate for each alloy and note the increase 12 plateau hardness for the stoichiometric alloy ( $\sim$ 2.5 GPa) vs. the Ni/Cr = 1/8 alloy ( $\sim$ 1.75 GPa). 13 However, the KJMA equation does not describe the hardening trends for the Cr-poor alloys (Ni/Cr = 2.2 and 2.4). For those alloys, the KJMA fits are reasonable fits to the highest 14 15 temperature data (475°C). However, in those datasets, the lowest temperature aging (373°C), 16 produces similar hardening to the intermediate temperature (418°C) as shown by the intermixing 17 for the black (373°C) and red (418°C) datapoints. While this observation is unexpected, it may 18 be consistent with the low temperature portion of the Ni-Cr phase diagram as put forth by Xiong 19 [5]. In that phase diagram, the Ni<sub>2</sub>Cr phase field is of finite width and extends concave 20 downward from 586°C and a Ni mole fraction of 0.667. Thus, it is possible that the two highest 21 aging temperatures lay in a two-phase field ( $Ni_2Cr + \gamma$ ), while the lowest aging temperatures are 22 in the single phase Ni<sub>2</sub>Cr region. Thus, the increased hardness at the lower aging temperature

could be the result of the position of the alloy in the phase diagram and not due to experimental scatter, error, or other hardening mechanism.

3

4

5

6

7

8

9

10

11

12

13

14

15

16

17

18

19

20

21

## 5 Summary

The role of stoichiometry on Ni-Cr ordering transformation was studied by microhardness and the extent of precipitation was confirmed by TEM and XRD. All of the alloys studies (Ni/Cr = 1.8, 2.0, 2.2, and 2.4) exhibited hardening due to the development of the long range ordered Ni<sub>2</sub>Cr phase. Characterization by TEM and XRD shows that hardening is a complex function of the size of ordered precipitates (p-size), the phase fraction and precipitation induced strain. For each stoichiometry studied, the extent of hardening is greatest at 475°C compared to the medium (418°C) and low (373°C) temperature microhardness data. The Ni/Cr=2.0 (33.24 at.% Cr) alloy exhibited the most extensive hardening due to precipitation of the ordered Ni<sub>2</sub>Cr phase and in general, the larger the deviation from stoichiometry the less hardening and ordering. Hardening, p-size, and strain behavior reaches a saturation point after 1,000 h ageing at 475°C, while the ordered fraction peaked near 500h and slightly decreased with longer aging times. The behavior at medium and low temperatures are more sluggish due to low diffusivities and is reasonable well captured by the KJMA model parameters for extrapolation to longer times and lower temperatures. While the KJMA equation fit the data for the Ni/Cr 1.8 and 2.0 alloys, deviation from the expected trends at low aging temperature in the Ni/Cr 2.2 and 2.4 alloys suggest that the Ni<sub>2</sub>Cr phase field may have significant curvature as indicated by Xiong.

## Acknowledgements

- 2 The authors want to acknowledge Dr. Alessandra Marucco et al. for their research on
- 3 stoichiometry and Dr. Bharat Gwalani et al. for the research of XRD on identifying ordered
- 4 structure. The previous research inspires author to perform the research in this paper. This
- 5 research is being performed using funding received from the DOE Office of Nuclear Energy's
- 6 Nuclear Energy University Program, Cooperative Agreement Number DE-NE0008423. This
- 7 material is also based upon work supported by the National Science Foundation under Grant No.
- 8 1653123-DMR. This work was supported by the U.S. Department of Energy, Office of Nuclear
- 9 Energy under DOE Idaho Operations Office Contract DE-AC07- 051D14517 as part of a
- 10 Nuclear Science User Facilities experiment. Use of the National Synchrotron Light Source-II,
- Brookhaven National Laboratory, was supported by the DOE under Contract No. DE-
- 12 SC0012704.

13

14

19

20

21

22

23

24

25

26

27

28

29

30

31

32

1

## References

- 15 [1] T. Allen, J. Busby, M. Meyer, D. Petti, Materials challenges for nuclear systems, Materials today 13(12) (2010) 14-23.
- 17 [2] T. Chester, S. Norman, C. William, Superalloys II, Eds. John Willey & Sons, Inc., New York (1976).
  - [3] K. Chiang, D. Dunn, G. Cragnolino, Effect of simulated groundwater chemistry on stress corrosion cracking of alloy 22, Corrosion 63(10) (2007) 940-950.
    - [4] F. Delabrouille, D. Renaud, F. Vaillant, J. Massoud, Long Range Ordering of Alloy 690, 14th Intl. Conference on Environmental Degradation of Materials in Nuclear Power Systems, Virginia Beach, VA, USA, 2009.
      - [5] W. Xiong, Thermodynamic and kinetic investigation of the Fe-Cr-Ni system driven by engineering applications, Department of Materials Science and Engineering, KTH Royal Institute of Technology, School of Industrial Engineering and Management, 2012.
      - [6] A. Marucco, Phase transformations during long-term ageing of Ni Fe Cr alloys in the temperature range 450–600° C, Materials Science and Engineering: A 194(2) (1995) 225-233.
    - [7] A. Marucco, Effects of composition on the order-disorder transformation in ni-cr based alloys, Key Engineering Materials, Trans Tech Publ, 1991, pp. 77-90.
    - [8] A. Marucco, B. Nath, Effects of Ordering on the Properties of Ni-Cr Alloys, Journal of Materials Science 23(6) (1988) 2107-2114.

```
1 [9] S. Lee, P. Nash, Phase diagrams of binary nickel alloys, ASM International, Materials Park
2 (OH) (1991) 133.
3 [10] X. Xie, Y. Zeng, L. Kou, J. Dong, L. Pike, D. Klarstrom, THE PRECIPITATION AND
```

- [10] X. Xie, Y. Zeng, L. Kou, J. Dong, L. Pike, D. Klarstrom, THE PRECIPITATION AND STRENGTHENING BEHAVIOR OF Ni2 (Mo, Cr) IN HASTELLOY® C-22HS® ALLOY, A NEWLY DEVELOPED HIGH MOLYBDENUM NI-BASE SUPERALLOY, (2008).
- [11] H.M. Tawancy, M.O. Aboelfotoh, High strength and high ductility in a nanoscale superlattice of Ni2(Cr,Mo) deformable by twinning, Scripta Materialia 59(8) (2008) 846-849.
- [12] G.A. Young, D.S. Morton, N. Lewis, R. Morris, J. Pyle, L. Barnard, R. Najafabadi, Effect of long range order on the stress corrosion susceptibility of a nickel-33 at% chromium alloy, Corrosion 72(11) (2016) 1433-1437.
  - [13] G. Young, D. Eno, Long range ordering in model Ni-Cr-X alloys, Fontevraud 8 Contribution of Materials Investigations and Operating Experience to LWRs' Safety, Performance and Reliability, France, Avignon, 2015.
- [14] E. Metcalfe, B. Nath, A. Wickens, Some effects of the ordering transformation in Nimonic 80A on stress relaxation behaviour, Materials Science and Engineering 67(2) (1984) 157-162.
- [15] K. Miyata, M. Igarashi, Effect of ordering on susceptibility to hydrogen embrittlement of a Ni-base superalloy, Metallurgical Transactions A 23(3) (1992) 953-961.
  - [16] F. Teng, J.D. Tucker, Role of Stoichiometry on Ordering in Ni-Cr Alloys, MRS Online Proceedings Library Archive 1809 (2015) 7-12.
- [17] F. Teng, L.-J. Yu, O. Ciuca, E. Marquis, G. Burke, J.D. Tucker, The Role of Stoichiometry on Ordering Phase Transformations in Ni–Cr Alloys for Nuclear Applications, Environmental Degradation of Materials in Nuclear Power Systems, Springer, 2017, pp. 251-259.
- [18] L. Barnard, G. Young, B. Swoboda, S. Choudhury, A. Van der Ven, D. Morgan, J. Tucker, Atomistic modeling of the order–disorder phase transformation in the Ni 2 Cr model alloy, Acta Materialia 81 (2014) 258-271.
- [19] J.D. Tucker, R. Najafabadi, T.R. Allen, D. Morgan, Ab initio-based diffusion theory and tracer diffusion in Ni–Cr and Ni–Fe alloys, Journal of Nuclear Materials 405(3) (2010) 216-234.
  [20] G.A. Young, J.D. Tucker, D.R. Eno, THE KINETICS OF LONG RANGE ORDERING IN NI-CR AND NI-CR-FE ALLOYS, (2013).
- [21] M. Song, Y. Yang, M. Wang, W. Kuang, C.R. Lear, G.S. Was, Probing long-range ordering in nickel-base alloys with proton irradiation, Acta Materialia 156 (2018) 446-462.
  - [22] S.D. Kiser, E. Hinshaw, J. Crum, L. Shoemaker, Nickel alloy welding requirements for nuclear service, Focus on Nuclear Power Generation 2005 (2005).
- [23] A. Marucco, Atomic ordering and  $\alpha'$  -Cr phase precipitation in long-term aged Ni3Cr and Ni2Cr alloys, Journal of materials science 30(16) (1995) 4188-4194.
- [24] J. Buršík, M. Svoboda, The existence of P phase and Ni2Cr superstructure in Ni-Al-Cr-Mo system, Scripta Materialia 39(8) (1998) 1107-1112.
- [25] M. Hirabayashi, M. Koiwa, K. Tanaka, T. Tadaki, T. Saburi, S. Nenno, H. Nishiyama, An experimental study on the ordered alloy Ni2Cr, Transactions of the Japan Institute of Metals 10(5) (1969) 365-371.
- [26] V. Kolotushkin, V. Kondrat'ev, A. Laushkin, V. Rechitskii, Effect of long-term aging on the structural and phase stability and properties of nickel-chromium alloys, Metal science and heat treatment 45(11) (2003) 411-414.
- [27] L. Guttman, Order-Disorder Phenomena in Metals, in: S. Frederick, T. David (Eds.), Solid State Physics, Academic Press1956, pp. 145-223.

[28] A. Marucco, Atomic ordering in the Ni Cr Fe system, Materials Science and Engineering: A 189(1) (1994) 267-276.

- [29] L. Karmazin, Lattice parameter studies of structure changes of Ni Cr alloys in the region of Ni2Cr, Materials Science and Engineering 54(2) (1982) 247-256.
  - [30] E. Frely, B. Beuneu, A. Barbu, G. Jaskierowicz, Investigation of ordering kinetics in Ni-Cr-Fe alloys under electron irradiation, Annales De Physique (1997).
    - [31] E. Frely, B. Beuneu, A. Barbu, G. Jaskierowicz, Short and Long-Range Ordering of (Ni 0.67 Cr 0.33) 1-x Fe x Alloys Under Electron Irradiation, MRS Proceedings, Cambridge Univ Press, 1996, p. 373.
    - [32] A. Arya, G.K. Dey, V.K. Vasudevan, S. Banerjee, Effect of chromium addition on the ordering behaviour of Ni–Mo alloy: experimental results vs. electronic structure calculations, Acta Materialia 50(13) (2002) 3301-3315.
    - [33] L. Karmazin, J. Krejčí, J. Zeman, γ Phase and Ni2Cr-type long-range order in Ni-rich NiCrMo alloys, Materials Science and Engineering: A 183(1-2) (1994) 103-109.
    - [34] P.S. Pao, S.J. Gill, C.R. Feng, D.J. Michel, Fatigue and fracture of a Ni2Cr ordered intermetallic alloy, Materials Science and Engineering: A 153(1) (1992) 532-537.
  - [35] B. Gwalani, T. Alam, C. Miller, T. Rojhirunsakool, Y.S. Kim, S.S. Kim, M.J. Kaufman, Y. Ren, R. Banerjee, Experimental investigation of the ordering pathway in a Ni-33 at.%Cr alloy, Acta Materialia 115 (2016) 372-384.
  - [36] A. Verma, J.B. Singh, N. Wanderka, J.K. Chakravartty, Delineating the roles of Cr and Mo during ordering transformations in stoichiometric Ni2(Cr1-x,Mox) alloys, Acta Materialia 96 (2015) 366-377.
  - [37] C. Pareige, F. Soisson, G. Martin, D. Blavette, Ordering and phase separation in Ni–Cr–Al: Monte Carlo simulations vs three-dimensional atom probe, Acta Materialia 47(6) (1999) 1889-1899.
    - [38] S. Meher, P. Nandwana, T. Rojhirunsakool, J. Tiley, R. Banerjee, Probing the crystallography of ordered Phases by coupling of orientation microscopy with atom probe tomography, Ultramicroscopy 148 (2015) 67-74.
  - [39] M. Sundararaman, L. Kumar, G.E. Prasad, P. Mukhopadhyay, S. Banerjee, Precipitation of an intermetallic phase with Pt 2 Mo-type structure in alloy 625, Metallurgical and Materials Transactions A 30(1) (1999) 41-52.
  - [40] X. Shi, S. Ghose, E. Dooryhee, Performance calculations of the X-ray powder diffraction beamline at NSLS-II, Journal of synchrotron radiation 20(2) (2013) 234-242.
  - [41] D.J. Sprouster, R. Weidner, S. Ghose, E. Dooryhee, T. Novakowski, T. Stan, P. Wells, N. Almirall, G. Odette, L. Ecker, Infrastructure development for radioactive materials at the NSLS-
    - II, Nuclear Instruments and Methods in Physics Research Section A: Accelerators, Spectrometers, Detectors and Associated Equipment 880 (2018) 40-45.
    - [42] F. Teng, Investigation of Thermal Degradation in Structural Alloys for Nuclear Power Systems, (2018).
  - [43] H.C. Pai, M. Sundararaman, B.C. Maji, A. Biswas, M. Krishnan, Influence of Mo addition on the solvus temperature of Ni2(Cr,Mo) phase in Ni2(Cr,Mo) alloys, Journal of Alloys and Compounds 491(1-2) (2010) 159-164.
  - [44] R. Hu, G.M. Cheng, J.Q. Zhang, J.S. Li, T.B. Zhang, H.Z. Fu, First principles investigation on the stability and elastic properties of Ni2Cr1-xMx (M = Nb, Mo, Ta, and W) superlattices, Intermetallics 33 (2013) 60-66.

1	[45] B.J. Berkowitz, C. Miller, The effect of ordering on the hydrogen embrittlement
2	susceptibility of Ni2Cr, Metallurgical Transactions A 11(11) (1980) 1877-1881.
3	[46] C.T. Sims, N.S. Stoloff, W.C. Hagel, superalloys II, Wiley New York1987.
4	[47] R. Kozubski, Long-range order kinetics in Ni3Al-based intermetallic compounds with L12-
5	type superstructure, Progress in materials science 41(1-2) (1997) 1-59.
6	[48] A.N. Kolmogorov, On the statistical theory of the crystallization of metals, Bull. Acad. Sci.
7	USSR, Math. Ser 1 (1937) 355-359.
8	[49] M. Avrami, Kinetics of phase change. III. Granulation, phase change, and microstructure, J.
9	chem. Phys 9(2) (1941) 177-184.
10	[50] M. Avrami, Kinetics of phase change. II transformation - time relations for random
11	distribution of nuclei, The Journal of Chemical Physics 8(2) (1940) 212-224.
12	[51] M. Avrami, Kinetics of phase change. I General theory, The Journal of chemical physics
13	7(12) (1939) 1103-1112.
14	[52] W.A. Johnson, R.F. Mehl, Reaction kinetics in processes of nucleation and growth, Trans.
15	Aime 135(8) (1939) 396-415.
16	
17	
1 /	

# 2 List of Figures

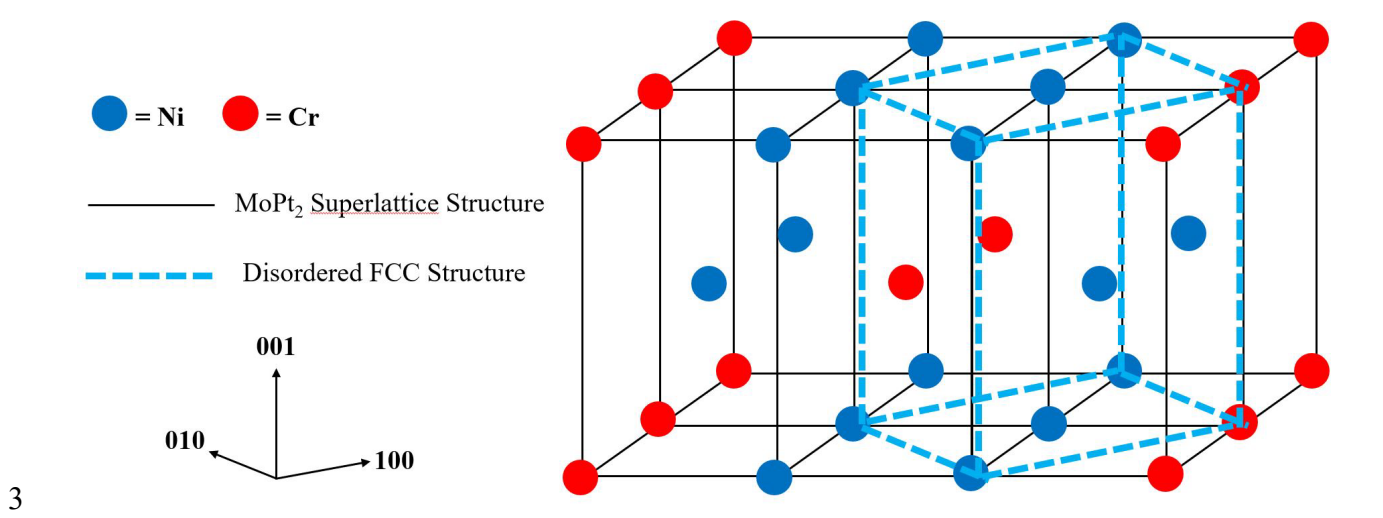


Figure 1. Schematic of MoPt<sub>2</sub> Superlattice Structure (Immm) in Ni-Cr (Fm-3m) System.

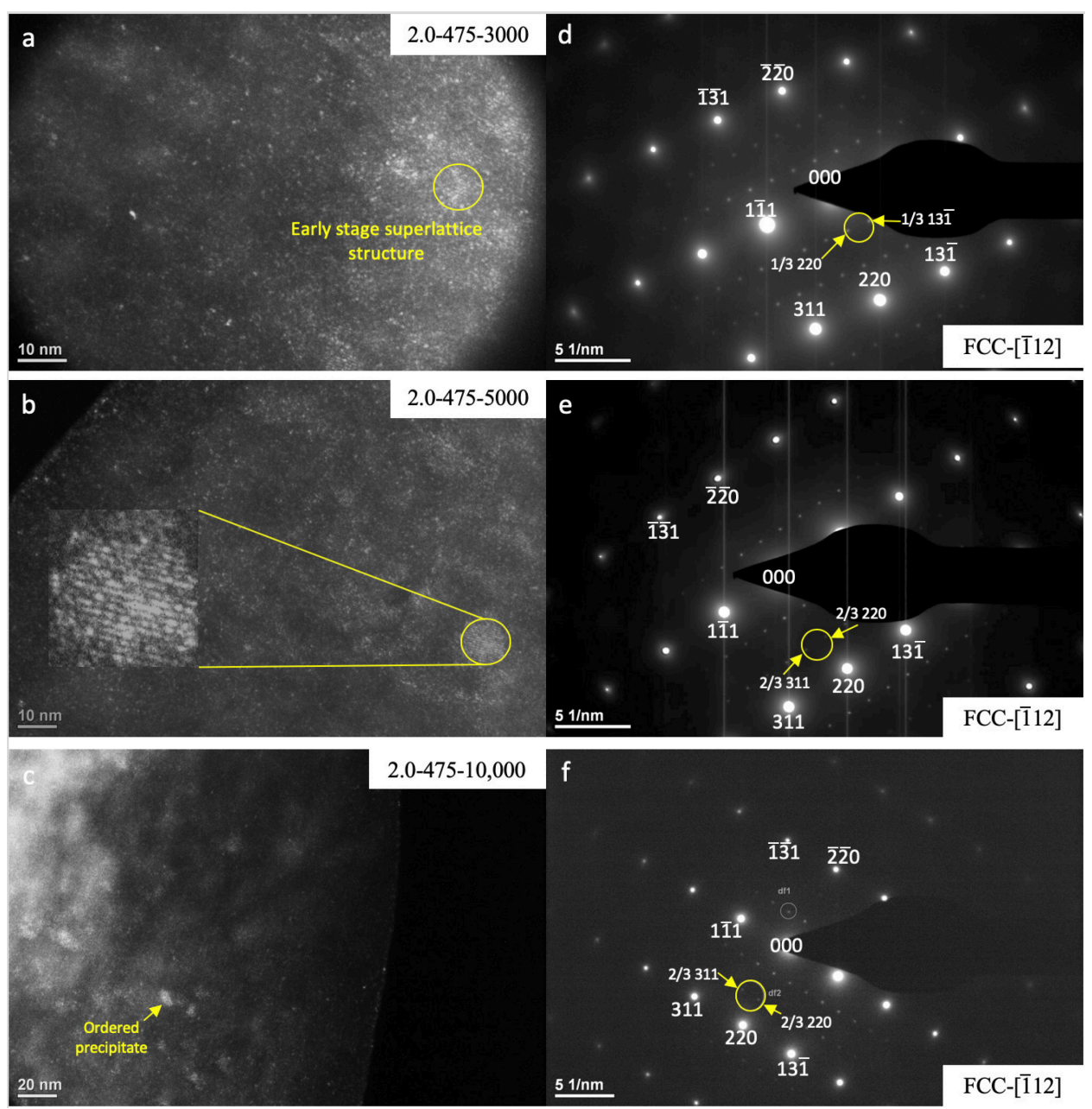


Figure 2. The evolution of ordering from 3000 to 10,000 h under TEM at [112] zone axis. (a) and (d) Darkfield image of Ni/Cr = 2.0 sample aged at  $475^{\circ}$ C for 3000 h and the corresponding diffraction pattern. (b) and (e) Darkfield image of Ni/Cr = 2.0 sample aged at  $475^{\circ}$ C for 5000 h and the corresponding diffraction pattern. The Ni2Cr superlattice structure is marked out and zoomed in. (c) and (f) Darkfield image of Ni/Cr = 2.0 sample aged at  $475^{\circ}$ C for 10,000 h and the corresponding diffraction pattern. Results shows that precipitation size for 3000 and 5000 h are similar, which is about 12 nm. The size of precipitation for 10,000 h aged sample is larger. Some precipitates are about 20 nm.

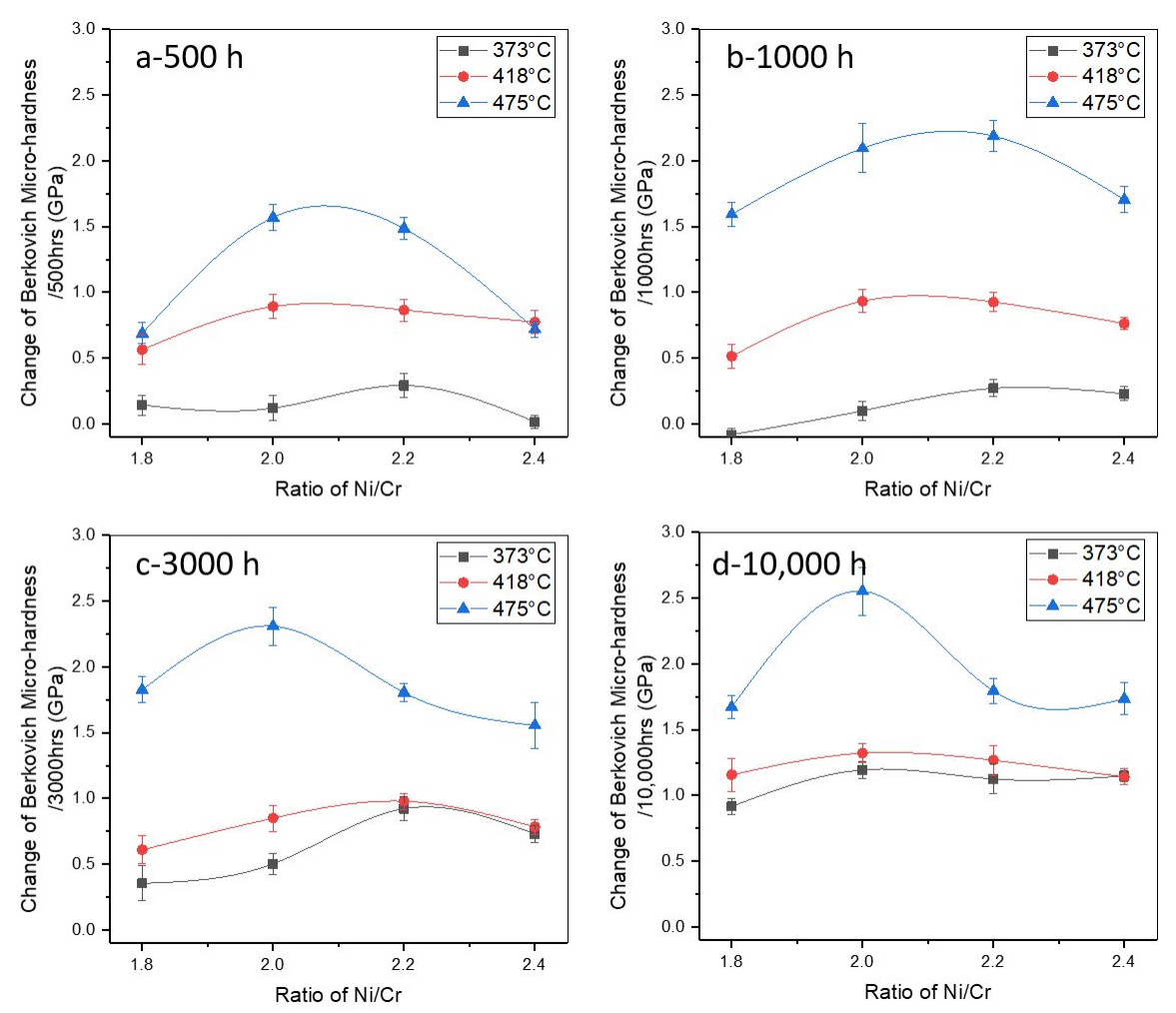


Figure 3. Change in microhardness as function of stoichiometry three temperatures when isothermal ageing comes to a) 500 h, b) 1000 h, c) 3000 h, and d) 10,000 h. The result shows that higher temperature is of earlier saturation on microhardness.  $475^{\circ}$ C starts showing the saturation behavior.  $373^{\circ}$ C and  $418^{\circ}$ C have not reached saturation point, but the faster kinetic can be observed at  $418^{\circ}$ C heat ageing. Ni/Cr = 2.0 samples are of highest value of change in hardness. Further distance from Ni/Cr = 2.0 causes smaller change in hardness.

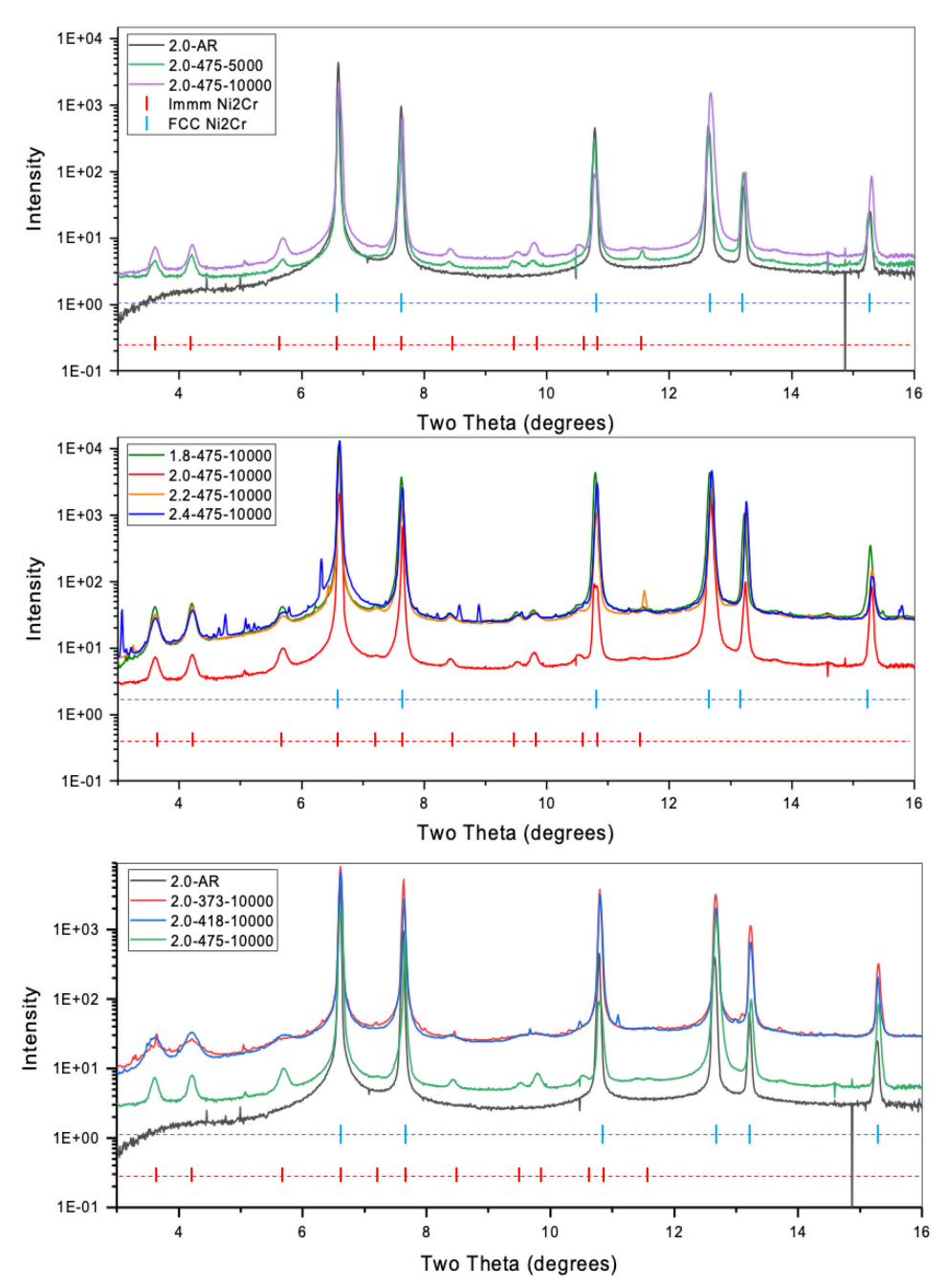


Figure 4. Synchrotron X-ray diffraction of Ni-Cr model alloys. Plot (a) indicates the evolution of ordering of Ni/Cr=2.0 alloy after aging at 475°C for 0, 5000, and 10,000 h. Phase identification is overlaid for the FCC matrix (blue ticks) and for the orthorhombic Ni<sub>2</sub>Cr phase (red ticks). Plot (b) indicates the evolution of ordering as a function of stoichiometry after 10,000 h ageing at 475°C. Plot (c) indicates the evolution of ordering as a function of ageing temperature on the Ni/Cr=2.0 alloy after aging 10,000 h. The peak broadening occurs as ageing temperature decreases, which indicates the changing of strain caused by ordered phase.

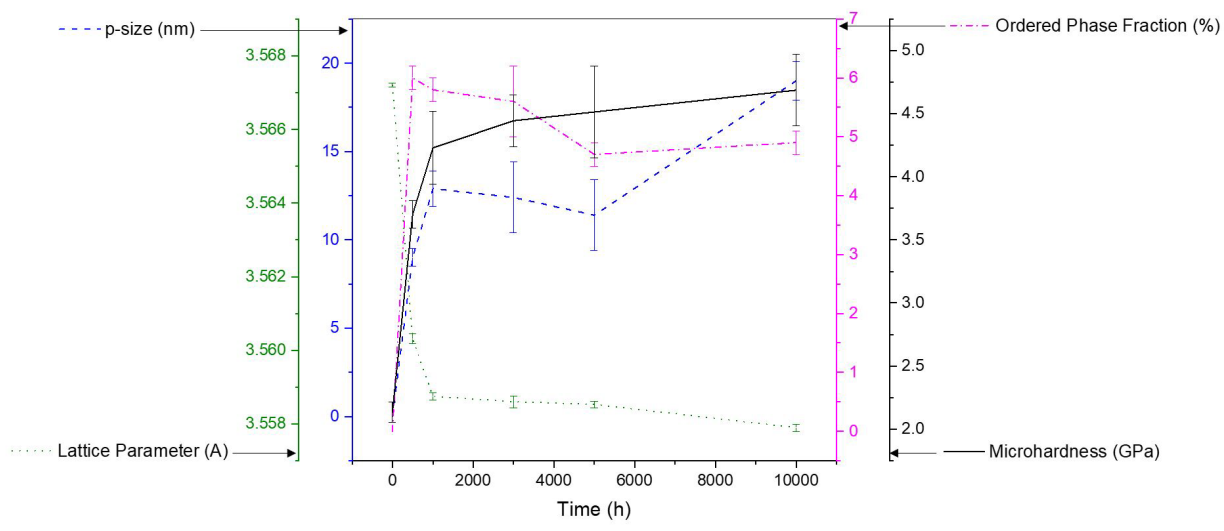


Figure 5. The evolution of p-size, lattice parameter, phase fraction, and microhardness as a function of ageing time. Sample and ageing condition: Ni/Cr = 2.0 samples at 475°C.

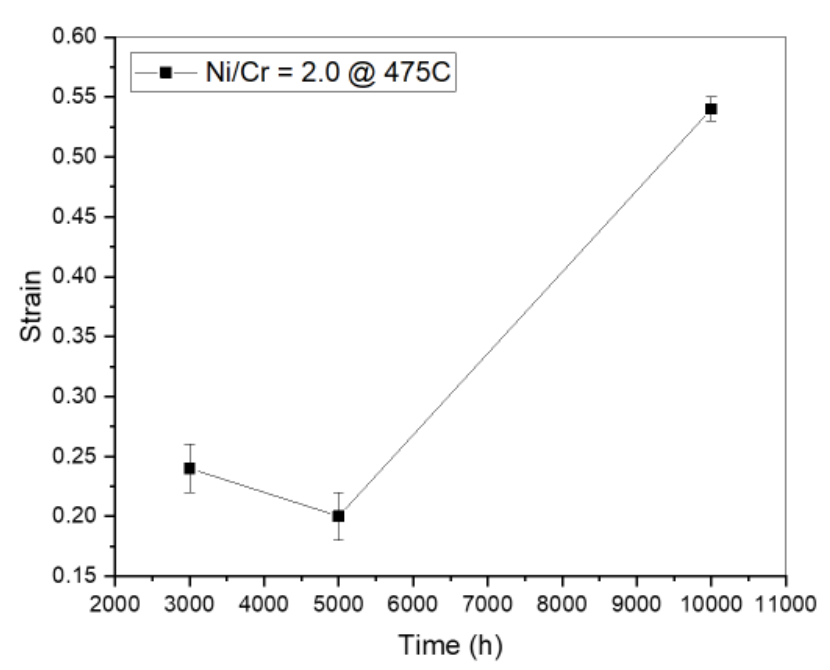


Figure 6. The growth of strain in sample Ni/Cr = 2.0 at 475°C from 3000 to 5000 h. Samples were prepared by jet polishing to remove the external induced strain.

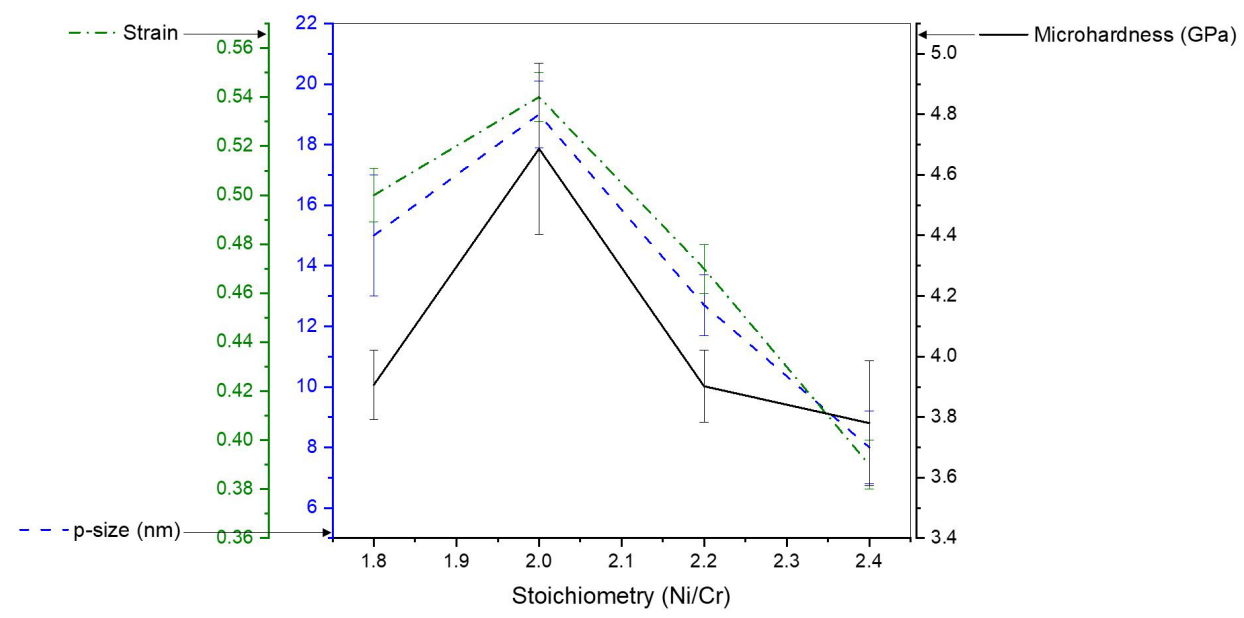


Figure 7. Role of stoichiometry on p-size, strain, and microhardness. Ageing condition: 10,000 h at 475°C.

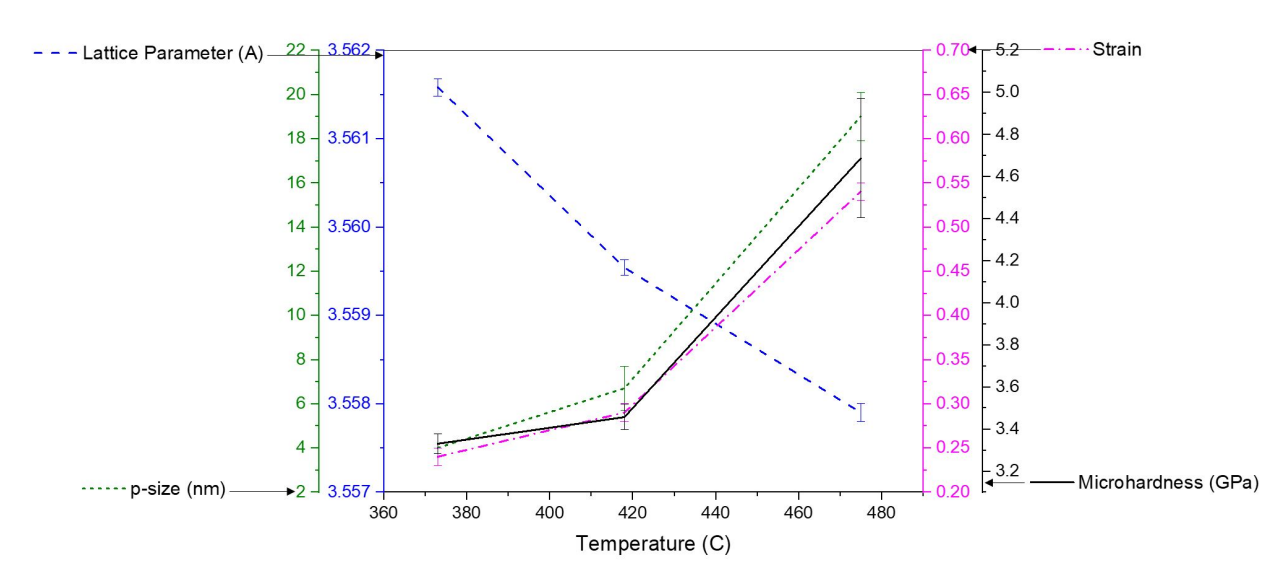


Figure 8. Role of temperature on lattice parameter, p-size, strain, and microhardness. Sample: Ni/Cr = 2.0. Ageing time is 10,000 h.

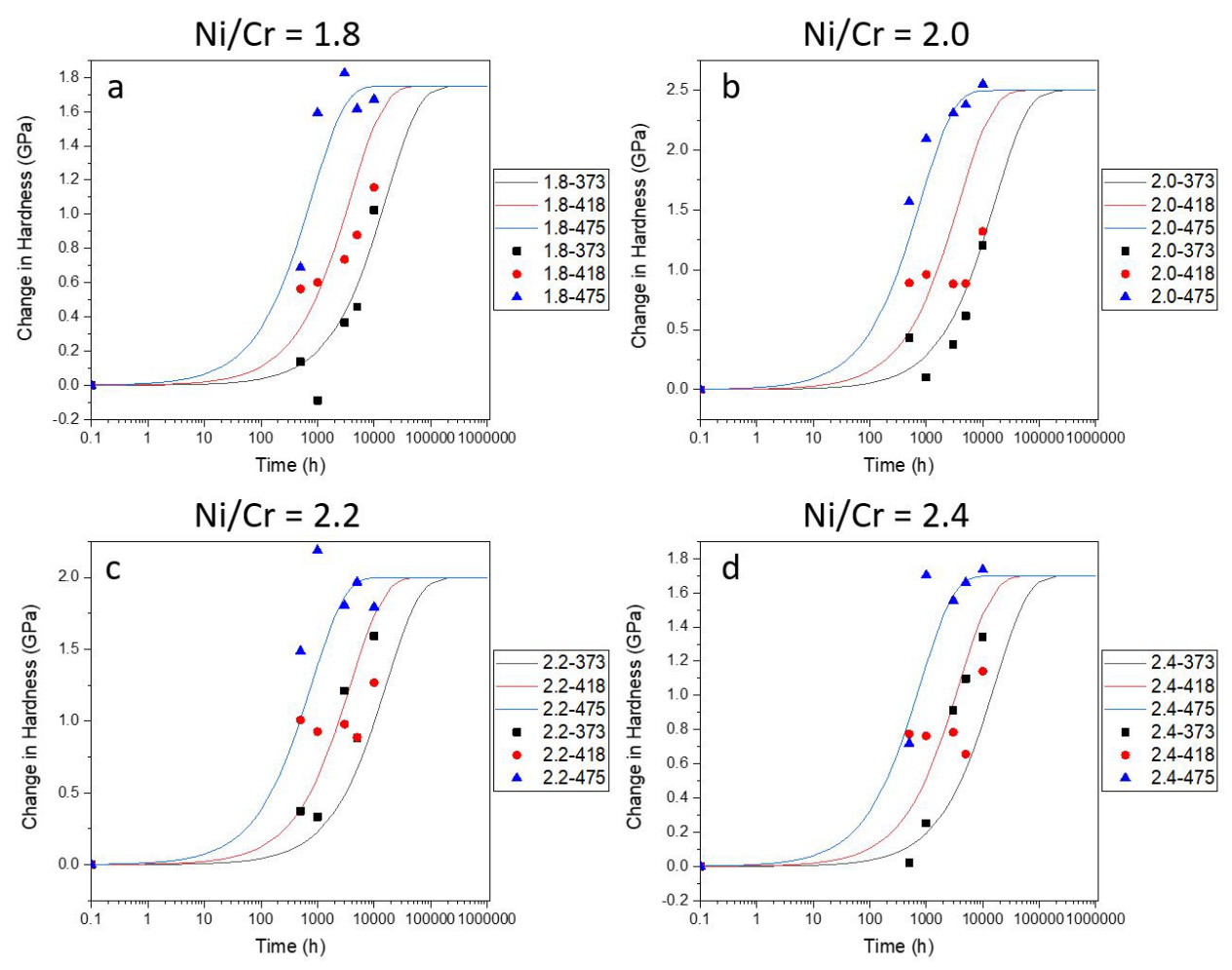


Figure 9. KJMA equation fitting result. (a) Ni/Cr = 1.8, (b) Ni/Cr = 2.0, (c) Ni/Cr = 2.2, (d) Ni/Cr = 2.4. Fitting parameters:  $k_0 = 3.00E + 05 \text{ h}^{-1}$ , Q = 120 kJ, n = 0.75.